PERGAMON

International Journal of Solids and Structures 39 (2002) 2965–2986

INTERNATIONAL JOURNAL OF SOLIDS and STRUCTURES

www.elsevier.com/locate/ijsolstr

Dynamic instability of a disk forced by a pulse of short duration

Michael El-Raheb *

1000 Oak Forest Lane, Pasadena, CA 91107, USA

Received 23 April 2001; received in revised form 24 March 2002

Abstract

A dynamic analysis is presented for circumferential buckling of a disk induced by transient axisymmetric flexural deformation from a pulse of short duration. A perturbation solution is adopted in solving the coupled non-linear stability equations, utilizing the asymmetric dynamic eigenfunctions of the disk as trial functions in the Galerkin procedure. Static buckling is treated first to demonstrate the utility of the stability analysis and evaluate how critical stress and circumferential wave number of the buckling mode depend on disk radius and thickness. In the dynamic case, transient response is the evolution in time of an axisymmetric deformation shape bounded by the shear wave front. Dynamic stability from induced inplane stresses of asymmetric perturbations is characterized by their divergence in time. The dynamic buckling mode is that mode growing fastest over a fixed period of time after impact. © 2002 Published by Elsevier Science Ltd.

Keywords: Dynamic; Instability; Buckling; Perturbation

1. Introduction

Observations of experiments on thin brittle disks and square plates struck centrally by a cylindrical projectile show a common mode of failure: cracking along radial lines with equiangular spacing which suggests a critical stress that varies periodically along the circumference with peaks along the radial cracks. Since the applied pressure from impact is axisymmetric, purely linear analysis predicts an axisymmetric response and fails to explain the asymmetry of the observed failure mode. The only phenomenon consistent with this mode of failure is dynamic instability growing from initial asymmetric imperfections along the perimeter of the disk or plate. The instability is caused by negative circumferential stress σ_θ induced by large flexural deformation.

Static buckling of a disk has been treated extensively in the literature. One of the earliest analytical treatments dates back to 1930, as quoted in Timoshenko and Woinowsky-Krieger's textbook (1959).

* Tel.: +1-626-796-5528; fax: +1-626-583-8834.
E-mail address: mertrident@earthlink.net (M. El-Raheb).

0020-7683/02/$ - see front matter © 2002 Published by Elsevier Science Ltd.
PII: S0020-7683(02)00258-5

Over 160,000 references treat static buckling of rectangular plates by the finite element method. Only 60 references treat buckling of a disk and among these, only three include inertial effects adopting a semi-analytical method. In these references, dynamics implies response from loading with periodic time dependence at a single frequency. None of these references considers analysis of buckling in a transient wave environment. From this list of references, there is space here to pick only a few representing various methods of solution. Bolotin's monogram on dynamic stability (Bolotin, 1956) presents a fundamental treatise on dynamic buckling of elastic systems. Chen and Juang (1987) and Bhushan et al. (1996) adopt finite elements to solve the non-linear and linearized stability equations. Tani and Yamaki (1981) treats stability and the effect on eigenfrequency of inplane stresses by the finite difference method. Yamaki et al. (1981), Laura et al. (1995), Shih et al. (1995), and Krizghevsky and Stavsky (1998) use the Galerkin method to determine stability in the frequency domain. Nath et al. (1985) adopts the Chebyshev collocation method to solve the static and free vibration stability equation. Turvey (1978), and Khadkhodayan et al. (1997) apply the method of dynamic relaxation to the buckling analysis for statics and free vibrations. Kolegov et al. (1991) studies experimentally how buckling deflection of disks changes with impulsive load for different diameters and thicknesses. This is the only reference reporting transient collapse.

In the analysis to be presented below, static buckling is treated by a linear perturbation solution of the coupled non-linear equations. The static axisymmetric flexural deformation $w_0(r)$ from applied pressure p acting over a concentric circular footprint is solved analytically adopting Mindlin's equations for a disk. The non-linear function in $w_0(r)$ and its derivatives forcing the inplane equilibrium equation yields the induced inplane stresses σ_r and σ_θ appearing in the stability equation governing the asymmetric displacement $w_n(r,\theta)$ where n is circumferential wave number. The asymmetric dynamic eigenfunctions of the disk serve as trial functions in a Galerkin solution. Critical pressure p_{cr} corresponds to that $n = n_{cr}$ for which buckling pressure $p(n)$ achieves a minimum.

The deformation of a disk forced by a pulse of short duration is confined by the shear wave front with instantaneous radius r_w. During the application of the external load, as r_w increases with time so does amplitude of the instantaneous deformed shape. As with static buckling, dynamic displacement induces a compressive σ_θ that causes displacement to diverge. The linear unsteady Mindlin's equations of the disk forced by the pressure pulse are solved by modal analysis. The resulting axisymmetric displacement $w_0(r,t)$ is utilized to compute σ_{r0} and $\sigma_{\theta 0}$. The time when the lowest eigenvalue vanishes marks the threshold of stability for some n. That n yielding the largest unstable growth of $\sigma_{\theta n}$ for some fixed elapsed time from impact determines the most dynamically unstable mode. Parameters important in static buckling, such as disk radius r_d, aspect ratio r_d/h where h is thickness, and modulus E, are now replaced by instantaneous radius of the wave front r_w, instantaneous aspect ratio r_w/h, and phase velocity c_p. Unlike the static case where critical $\sigma_{\theta n}$ occurs near the edge, in the dynamic case critical $\sigma_{\theta n}$ may occur at $r_w < r_d$. In turn, $w_0(r,t)$ must reach larger values than in statics to attain the threshold of stability.

Sections 1.1 and 1.2 formulate the pre-buckling axisymmetric state and the asymmetric stability equation for static buckling and dynamic instability. Section 2 discusses the sensitivity of p_{cr} to r_d and h for a static problem, and extends the results to wave propagation explaining how it differs from the simpler static problem.

1.1. Static analysis

When a thin disk is loaded axisymmetrically, lateral displacement w_0 from flexure induces inplane stresses σ_{r0} and $\sigma_{\theta 0}$. If the disk boundary is stress free in its plane, $\sigma_{\theta 0}$ changes from tensile near the disk center to compressive near its boundary (see Timoshenko and Woinowsky-Krieger, 1959). Except for a disk fully clamped along the perimeter, this reversal of $\sigma_{\theta 0}$ along r occurs for both free and simply supported boundaries. The compressive $\sigma_{\theta 0}$ may buckle the disk along the perimeter.

Consider the inplane static equilibrium equation for axisymmetric deformation

$$\frac{\partial \sigma_{r0}}{\partial r} + \frac{\sigma_{r0} - \sigma_{\theta 0}}{r} = 0 \tag{1}$$

For plane strain, the constitutive law simplifies to

$$\sigma_{r0} = \frac{E}{1-v^2}\left(u_0' + \frac{1}{2}(w_0')^2 + \frac{v u_0}{r}\right) \tag{2a}$$

$$\sigma_{\theta 0} = \frac{E}{1-v^2}\left(v u_0' + \frac{v}{2}(w_0')^2 + \frac{u_0}{r}\right) \tag{2b}$$

where u_0 is radial displacement and $(\ )'$ stands for partial derivative with respect to variable r. The term $(1/2)(w_0')^2$ is the non-linear radial strain coupling transverse to inplane variables. Substituting (2a) and (2b) in (1) yields

$$\nabla_1^2 u_0 \equiv u_0'' + \frac{1}{r}u_0' + \frac{u_0}{r^2} = -\left(w_0' w_0'' + \frac{1-v}{2}\frac{w_0'^2}{r}\right) \tag{3}$$

In-plane stresses $(\sigma_{r0}, \sigma_{\theta 0})$ multiplied by curvature produce non-linear shear terms modifying the w equilibrium equation to

$$D\nabla^4 w - h\sigma_{r0} w'' - h\sigma_{\theta 0}\left(\frac{1}{r}w' + \frac{1}{r^2}\frac{\partial^2 w}{\partial \theta^2}\right) = p[H(r) - H(r - r_p)] \tag{4}$$

$$\nabla^4 \equiv \left(\frac{\partial^2}{\partial r^2} + \frac{1}{r}\frac{\partial}{\partial r} + \frac{1}{r^2}\frac{\partial^2}{\partial \theta^2}\right)^2, \quad D = \frac{Eh^3}{12(1-v^2)}$$

where $H(r)$ is the Heaviside function and θ is the circumferential angle. The coupled non-linear Eqs. (3) and (4) in u_0 and w govern the stability of the disk.

An axisymmetric load applied to an axisymmetric geometry cannot induce circumferentially asymmetric modes. Asymmetry may result either from loading or geometric imperfections p_i and w_i. Magnification of these asymmetric perturbations with applied load is the basis of bifurcation from an almost axisymmetric response to an asymmetric instability. Let $p(r, \theta, t)$ be the total applied forcing pressure made of an axisymmetric part p_0 of order unity and an asymmetric part p_i of much smaller magnitude. Also let w_i be the geometric imperfection. For simplicity, consider a Fourier expansion of p_i and w_i in terms of circumferential harmonics

$$\begin{aligned} &p(r, \theta, t) = (p_0 + p_i(\theta)) f_p(t) \\ &p_i(\theta) = \varepsilon_p \sum_{n=2}^{N} \cos(n\theta), \quad w_i(r, \theta) = \varepsilon_w r \sum_{n=2}^{N} \cos(n\theta) \end{aligned} \tag{5}$$

where $f_p(t)$ is time dependence of p and equals unity for a static problem, and ε_p and ε_w are magnitudes of loading and geometric imperfections so that $\varepsilon_p \ll p_0$, $\varepsilon_w = o(w_0)$. Since an $n = 0$ imperfection does not induce asymmetry, and since an $n = 1$ imperfection corresponds to a rigid body translation or rotation, only harmonics with $n \geqslant 2$ are included in the expansions of Eq. (5). In practice, the geometric imperfection in a disk is larger at the perimeter than it is near the center. Also, continuity of w_i at $r = 0$ for $n > 0$ requires it to vanish there. The simplest radial function meeting these two requirements is linear with r as described in Eq. (5). Both ε_p and ε_w are assumed to have the same magnitude for all circumferential harmonics. This choice which assumes equal weight of all loading imperfections will show if the unstable mode has a preferential n.

Numerical solution of the set (3) and (4) determines p as a function of w. An instability occurs when the slope of the line p versus w becomes negative, indicating that strain energy ceases to be positive definite. Another way to determine critical pressure p_{cr} is to solve the non-linear set (3) and (4) adopting a linearized perturbation method. Express (u, w) as the sum of an axisymmetric term of $O(1)$ and an asymmetric term of order $o(\varepsilon)$

$$\begin{aligned} u(r,\theta) &= u_0(r) + u_n(r)\sin n\theta \\ w(r,\theta) &= w_0(r) + w_n(r)\cos n\theta \end{aligned} \tag{6}$$

where n is an integer circumferential wave number. Substituting (6) in (3) and (4) and equating terms of the same order of smallness in ε yields

$$D\nabla_0^4 w_0 = p_0[H(r) - H(r - r_p)] \tag{7a}$$

$$\nabla_1^2 u_0 = -\left(w_0' w_0'' + \frac{1-\nu}{2}\frac{(w_0')^2}{r}\right) \equiv -W_0(w_0(r)) \tag{7b}$$

$$\begin{aligned} &D\nabla_n^4 w_n - G(\sigma_0, w_n) = \varepsilon_p + \varepsilon_w G(\sigma_0, r) \\ &G(\sigma_0, w_n) = h\left[\sigma_{r0} w_n'' + \sigma_{\theta 0}\left(\frac{w_n'}{r} - n^2\frac{w_n}{r^2}\right)\right] \end{aligned} \tag{7c}$$

$$\nabla_n^2 \equiv \frac{\partial^2}{\partial r^2} + \frac{1}{r}\frac{\partial}{\partial r} - \frac{n^2}{r^2}, \quad \nabla_n^4 \equiv \nabla_n^2 \nabla_n^2$$

where the right hand side of (7c) is a known forcing term. The functional $G(\sigma_0, w_n)$ is geometric stiffness from asymmetric displacement, and $G(\sigma_0, r)$ is geometric stiffness from initial imperfection. These account for shear forces produced by initial axisymmetric stresses acting on curvature from asymmetric displacement and geometric imperfection. Eq. (7a) governs the pre-buckling static axisymmetric displacement $w_0(r)$ from the applied pressure p. Once w_0 is determined, the functional W_0 becomes a known function of r. Substituting $W_0(w_0(r))$ in (7b) and expressing ∇_1^2 as

$$\nabla_1^2 u_0 \equiv \frac{\partial}{\partial r}\left(\frac{1}{r}\frac{\partial}{\partial r}(r u_0)\right) \tag{7d}$$

then integrating (7a) yields $u_0(r)$

$$u_0(r) = -\frac{1}{r}\int_0^r \eta \int_0^\eta W_0(\xi)\,\mathrm{d}\xi\,\mathrm{d}\eta + C_1 r + C_2/r \tag{8}$$

where C_1, C_2 are constants of integration. C_2 drops out because the solution is bounded at $r = 0$. Substituting (8) into (2a) and (2b) produces

$$\sigma_{r0}(r) = \frac{E}{1-\nu^2}\left\{\frac{(1-\nu)}{r^2}\int_0^r \eta \int_0^\eta W_0(\xi)\,\mathrm{d}\xi\,\mathrm{d}\eta - \int_0^r W_0(\xi)\,\mathrm{d}\xi + \frac{1}{2}(w_0'(r))^2 + (1+\nu)C_1\right\} \tag{9a}$$

$$\sigma_{\theta 0}(r) = \frac{E}{1-\nu^2}\left\{-\frac{(1-\nu)}{r^2}\int_0^r \eta \int_0^\eta W_0(\xi)\,\mathrm{d}\xi\,\mathrm{d}\eta - \nu\int_0^r W_0(\xi)\,\mathrm{d}\xi + \frac{\nu}{2}(w_0'(r))^2 + (1+\nu)C_1\right\} \tag{9b}$$

Evaluating (9a) at $r = r_d$ and equating to zero for a stress-free boundary determines C_1

$$(1+\nu)C_1 = -\frac{(1-\nu)}{r_d^2}\int_0^{r_d} \eta \int_0^\eta W_0(\xi)\,\mathrm{d}\xi\,\mathrm{d}\eta + \int_0^{r_d} W_0(\xi)\,\mathrm{d}\xi - \frac{1}{2}(w_0'(r_d))^2 \tag{9c}$$

Substituting (9c) in (9b) yields the expression for $\sigma_{\theta 0}(r)$

$$\sigma_{\theta 0}(r) = \frac{E}{1-v^2}\left\{ -\frac{(1-v)}{r^2}\int_0^r \eta \int_0^\eta W_0(\xi)\,\mathrm{d}\xi\,\mathrm{d}\eta - v\int_0^r W_0(\xi)\,\mathrm{d}\xi + \frac{v}{2}(w_0'(r))^2 - \frac{(1-v)}{r_\mathrm{d}^2}\int_0^{r_\mathrm{d}} \eta \int_0^\eta W_0(\xi)\,\mathrm{d}\xi\,\mathrm{d}\eta + \int_0^{r_\mathrm{d}} W_0(\xi)\,\mathrm{d}\xi - \frac{1}{2}(w_0'(r_\mathrm{d}))^2 \right\} \tag{9d}$$

Since $\mathrm{d}^k w_0/\mathrm{d}r^k$ is proportional to p, and $(\sigma_{r0}, \sigma_{\theta 0})$ are proportional to $(\mathrm{d}^k w_0/\mathrm{d}r^k)^2$, then expressing $\sigma_0 = \hat{\sigma}_0 p_0^2$ brings p_0 explicitly in Eq. (7c)

$$D\nabla_n^4 w_n - p_0^2 G(\hat{\sigma}_0, w_n) = \varepsilon_p + \varepsilon_w G(\hat{\sigma}_0, r) \tag{10a}$$

Approximating w_n by trial functions φ_{nj}

$$w_n(r) = \sum_j C_{nj}\varphi_{nj}(r) \tag{10b}$$

then substituting (10b) in (10a), multiplying both sides by $r\varphi_{nk}(r)$ and integrating over the domain produces the matrix equation

$$[\mathbf{M}_{1n} - \mathbf{M}_{2n}\mathbf{I}p_0^2]\mathbf{C}_n = \mathbf{R}_{np}\varepsilon_p + \mathbf{R}_{nw}\varepsilon_w \tag{10c}$$

$$M_{1njk} = \int_0^{r_\mathrm{d}} D\nabla_0^4(\varphi_{nj})\varphi_{nk} r\,\mathrm{d}r, \quad R_{npk} = \int_0^{r_p} \varphi_{nk}(r) r\,\mathrm{d}r$$

$$M_{2njk} = \int_0^{r_\mathrm{d}} G(\hat{\sigma}_0, \varphi_{nj})\varphi_{nk} r\,\mathrm{d}r, \quad R_{nwk} = \int_0^{r_\mathrm{d}} G(\hat{\sigma}_0, r) r\,\mathrm{d}r$$

$$\Rightarrow \mathbf{C}_n = [\mathbf{M}_{1n} - \mathbf{M}_{2n}\mathbf{I}p_0^2]^{-1}(\mathbf{R}_{np}\varepsilon_p + \mathbf{R}_{nw}\varepsilon_w)$$

The weight $r\varphi_{nk}(r)$ is used instead of $\varphi_{nk}(r)$ alone consistent with cylindrical coordinates and the fact that if $\varphi_{nk}(r)$ were a set of orthogonal eigenfunctions then orthogonality may be utilized to simplify calculations. In (10c) $\mathbf{C}_n$ diverges at characteristic values of p_0 for which

$$\det|\mathbf{M}_{1n} - \mathbf{M}_{2n}\mathbf{I}p_0^2| = 0 \tag{10d}$$

yielding the critical pressure p_cr as the smallest eigenvalue of (10d).

The concept of functional form is presented below. The solution to a system of linear ordinary differential equations can be expressed as the sum of primitives which are functions of the independent variables and parameters, multiplied by coefficients that depend only on the parameters. If the primitives are independent of the parameters and all coefficients share the same dependence on these parameters, then the functional form of the solution is independent of the parameters. This means that the normalized shape of the solution is independent of the parameters while its magnitude may vary by a constant multiplicative factor. This definition may be cast in mathematical form as

$$S(\alpha_i, x_m) = C(\alpha_i)\sum_j \beta_j P_j(k_m x_m) \tag{11}$$

where $S(\alpha_i, x_m)$ is the solution function, α_i are the parameters, x_m are the independent variables, $C(\alpha_i)$ is a function of parameters only, β_j are constants, and $P_j(k_m x_m)$ are primitives of the differential operator and are functions of constants k_m and x_m. The functional form of the solution given by Eq. (11) is independent of α_i.

Consider the following two forms for $w_0(r)$ in (7a) and (7b):

1. the approximation $w_0(r) = J_0(k_0 r)$ where $J_0''(k_0 r_d) = 0$ is a non-natural boundary condition approximating simple supports,
2. the static axisymmetric displacement $w_0(r)$ satisfying (7a) (see Appendix A),

where $J_m(k_m r)$, $m = 0, 1$ is the Bessel function and k_m is radial wave number. Similarly, consider the following two forms for $w_n(r,\theta)$ in (7c):

1. the approximation $w_n(r,\theta) = \cos(n\theta) J_n(k_n r)$ where $J_n''(k_n r_d) = 0$ approximates the same boundary condition as that for $w_0(r)$,
2. the asymmetric eigenfunctions of the homogeneous dynamic Mindlin's equations (see Appendix B).

Substituting the one-term approximations above in Eqs. (7a)–(7c) yields

$$w_0(r) = p_{cr} \frac{\int_0^{r_p} J_0(k_0 r) r \, dr}{D k_0^4 \int_0^{r_d} J_0^2(k_0 r) r \, dr} J_0(k_0 r) \tag{12a}$$

$$p_{cr} = \frac{D k_n^4 \int_0^{r_d} J_n^2(k_n r) r \, dr}{\int_0^{r_d} g(r) J_n(k_n r) r \, dr} \tag{12b}$$

$$g(r) = h\sigma_{r0} k_n^2 J_n''(k_n r) + h\sigma_{\theta 0}\left(\frac{k_n}{r} J_n'(k_n r) - \frac{n^2}{r^2} J_n(k_n r)\right) \tag{12c}$$

where $J_n'(k_n r)$ is derivative with respect to the argument $(k_n r)$. Applying dimensional analysis to Eqs. (12a)–(12c) reveals that

$$p_{cr} \propto \frac{E h^4}{r_d^2 r_p^2} \tag{12d}$$

Clearly, the explicit dependence on r_d/h and r_p/r_d of w_0 in (12a), u_0 in (7b) and $(\sigma_{r0}, \sigma_{\theta 0})$ in (9a) and (9d), renders the functional form of $(\sigma_{r0}, \sigma_{\theta 0})$ independent of r_d/h and r_p/r_d while magnitude is within a multiplicative scaling factor σ_0:

$$\sigma_0 = \frac{E}{(1-\nu^2)} \frac{p_0^2}{(D k_0^4 r_d)^2} \tag{12e}$$

Since n of the critical mode depends primarily on the functional form of $(\sigma_{r0}, \sigma_{\theta 0})$, it also is independent of r_d/h and r_p/r_d. Consequently, the one-term approximation predicts that n of the buckling mode is independent of r_d/h and r_p/r_d.

Express $w_n(r,\theta)$ in terms of the dynamic eigenfunctions of the disk (See Appendix B)

$$w_n(r,\theta) = \cos n\theta \sum_j d_j \varphi_{nj}(r) \tag{13}$$

Substituting (13) into (7c), then eliminating the r dependence by multiplying (7c) by $r\varphi_{nk}(r)$ and integrating from zero to r_d yields

$$\mathbf{M}_n \mathbf{d} = \mathbf{R}_0 \tag{14a}$$

$$M_{njk} = F_{njk} - G_{njk} \tag{14b}$$

$$F_{njk} = D\int_0^{r_d} \nabla_n^4(\varphi_{nj})\varphi_{nk} r\,\mathrm{d}r$$
$$G_{njk} = h\int_0^{r_d} \left[\sigma_{r0}\varphi''_{nj} + \sigma_{\theta 0}\left(\frac{1}{r}\varphi'_{nj} - \frac{n^2}{r^2}\varphi_{nj}\right)\right]\varphi_{nk} r\,\mathrm{d}r \tag{14c}$$

$$R_{0k} = h\int_0^{r_d} \left(\sigma_{r0} w''_0 + \sigma_{\theta 0}\frac{w'_0}{r}\right)\varphi_{nk} r\,\mathrm{d}r \tag{14d}$$

From (B.22c), $\varphi_{nj}(r)$ in (14c) and (14d) takes the form

$$\varphi_n(r) = \sum_{j=1}^{2} C_{nj} J_n(k_{nj} r) \quad \text{(see (B.22c))}$$

$$\Rightarrow \nabla_n^4 \varphi_n(r) = \sum_{j=1}^{2} C_{nj} k_{nj}^4 J_n(k_{nj} r) \tag{14e}$$

The critical pressure is reached when p_0^2 factoring σ_{r0} and $\sigma_{\theta 0}$ in (14d) is the smallest eigenvalue of

$$\det|\mathbf{M}_n| = 0 \tag{14f}$$

1.2. Dynamic analysis

In the dynamic case, $w_0(r,t)$ is determined adopting a modal solution to the axisymmetric Mindlin's equation (see El-Raheb and Wagner (1987))

$$w_0(r,t) = \sum_j a_j(t)\varphi_{0j}(r) \tag{15a}$$

$$a_j(t) = -\frac{N_{fj}}{\omega_j N_{0j}}\int_0^t f_p(\tau)\sin\omega_j(t-\tau)\,\mathrm{d}\tau \tag{15b}$$

where $\{\omega_j, \varphi_{0j}\}$ is the eigenset, $f_p(t)$ is defined in Eq. (5), and

$$N_{fj} = p_0\int_0^{r_p} \varphi_{0j}(r) r\,\mathrm{d}r, \quad N_{0j} = \int_0^{r_d}\left[\varphi_{0j}^2(r) + \frac{h^2}{12 r_d^2}\eta_{0j}^2(r)\right] r\,\mathrm{d}r$$

At every time step t, $w_0(r,t)$, determined from (15a) and (15b), forms the instantaneous functional $W_0[w_0(r,t)]$.

The dynamic counterpart of (7b) is

$$\nabla_1^2 u_0 - \frac{1}{c_\varepsilon^2}\frac{\partial^2 u_0}{\partial t^2} = -W_0(r,t), \quad c_\varepsilon = \sqrt{\frac{E}{\rho(1-\nu^2)}} \tag{16}$$

Expressing $u_0(r,t)$ in terms of its eigenset $\{\bar{\omega}_j, J_1(\gamma_j r)\}$

$$u_0(r,t) = \sum_j c_j(t) J_1(\gamma_j r), \quad \gamma_j = \frac{\bar{\omega}_j}{c_\varepsilon} \tag{17a}$$

The stress-free boundary condition $\sigma_{r0}(r_d) = 0$ imposes the dispersion relation

$$(\gamma_j r_d) J_1'(\gamma_j r_d) + \nu J_1(\gamma_j r_d) = 0 \tag{17b}$$

which determines the eigenvalues $\bar{\omega}_j$. Substituting (17a) in (16) and exploiting orthogonality of $J_1(\gamma_j r)$ yields

$$\ddot{c}_j + \bar{\omega}_j^2 c_j = \frac{\overline{N}_{uj}(t)}{\overline{N}_{0j}} \tag{18}$$

$$\overline{N}_{uj}(t) = \int_0^{r_d} W_0(r,t) J_1(\gamma_j r) r \,\mathrm{d}r, \quad \overline{N}_{0j} = \frac{1}{c_\varepsilon^2} \int_0^{r_d} J_1^2(\gamma_j r) r \,\mathrm{d}r$$

Eq. (18) admits a solution

$$c_j(t) = -\frac{1}{\bar{\omega}_j \overline{N}_{0j}} \int_0^t \sin \bar{\omega}_j (t-\tau) \overline{N}_{uj}(\tau) \,\mathrm{d}\tau \tag{19}$$

which determines $u_0(r,t)$ from (17a) and subsequently σ_{r0} and $\sigma_{\theta 0}$ from (2a) and (2b).

The procedure for determining the threshold of dynamic stability is now outlined. Start with the dynamic counterpart of (7c) (see Eq. (B.4))

$$D\left[\left(\nabla_n^2 - \frac{1}{c_\varepsilon^2}\frac{\partial^2}{\partial t^2}\right)\left(\nabla_n^2 - \frac{1}{c_s^2}\frac{\partial^2}{\partial t^2}\right) + \frac{12}{c_\varepsilon^2 h^2}\frac{\partial^2}{\partial t^2}\right] w_n - G(\sigma_0, w_n) = \varepsilon_p f_p(t) + \varepsilon_w G(\sigma_0, r) \tag{20}$$

From Eq. (5), the asymmetric loading imperfection ε_p follows the same functional dependence on t as p_0. Assume the eigenset $\{\varphi_{nj}, \eta_{rnj}, \eta_{\theta nj}\}$ derived in Appendix B as trial functions to solve w_n in Eq. (20)

$$w_n(r,t) = \sum_j d_{nj}(t) \varphi_{nj}(r) \tag{21}$$

Substituting (21) in (20), then eliminating the r dependence by exploiting orthogonality of the eigenset yields

$$\mathbf{N}_n(\ddot{\mathbf{d}}_n + \mathbf{I}\omega_n^2 \mathbf{d}_n) - \mathbf{H}_n(t)\mathbf{d}_n = \mathbf{R}_{np}\varepsilon_p f_p(t) + \mathbf{R}_{nw}\varepsilon_w \tag{22a}$$

where $\dot{(\ )}$ is derivative with respect to time, ω_n are the eigenvalues of the axisymmetric problem in Eqs. (15a) and (15b) and

$$N_{njk} = \rho h \delta_{jk} \int_0^{r_d} \left[\varphi_{nj}^2 + \frac{h^2}{12}(\eta_{rnj}^2 + \eta_{\theta nj}^2)\right] r \,\mathrm{d}r \tag{22b}$$

$$H_{njk}(t) = \int_0^{r_d} G(\sigma_0, \varphi_{nj}) \varphi_{nk} r \,\mathrm{d}r, \quad R_{npk} = \int_0^{r_p} \varphi_{nk} r \,\mathrm{d}r, \quad R_{nwk} = \int_0^{r_d} G(\sigma_0, r) \varphi_{nk} r \,\mathrm{d}r$$

where δ_{jk} is the Kronecker delta. Combining coefficients of $\mathbf{d}_n$ in (22a) yields

$$\ddot{\mathbf{d}}_n + [\mathbf{I}\omega_n^2 - \mathbf{N}_n^{-1}\mathbf{H}_n(t)]\mathbf{d}_n = \mathbf{N}_n^{-1}[\mathbf{R}_{np}\varepsilon_p f_p(t) + \mathbf{R}_{nw}\varepsilon_w] \tag{23}$$

$\mathbf{H}_n(t)$ is a time-dependent geometric stiffness matrix. The coupled Eq. (23) describe the evolution of the asymmetric mode with n circumferential waves. For some fixed $t = t_{cr}$, Eq. (23) become unstable when one or more components of the instantaneous eigenvalue $\hat{\boldsymbol{\omega}}_n(t_{cr})$ vanish,

$$\hat{\boldsymbol{\omega}}_{nk}(t_{cr}) = 0, \quad k = k_{cr} \tag{24a}$$

where k is radial wave number. $\hat{\boldsymbol{\omega}}_n(t)$ diagonalizes (23) and satisfies the time-dependent eigenvalue problem

$$\mathbf{I}\hat{\boldsymbol{\omega}}_n^2(t) - [\mathbf{I}\omega_n^2 - \mathbf{N}_n^{-1}\mathbf{H}_n(t)] = \mathbf{0} \tag{24b}$$

Condition (24a) is the onset of dynamic instability. Since $(\sigma_{r0}, \sigma_{\theta 0})$ in $\mathbf{H}_n(t)$ are time-dependent and rise with $w_0(t)$, more than one mode will become unstable while the forcing function acts. This means that for each (n,k) dyad, a t_{cr} is reached when (24a) is satisfied. The growth of the unstable modes with time is according

to the solution of the coupled Eq. (23) for each n. That mode growing fastest corresponds to the dominant asymmetric dynamic buckling mode with n_{cr} circumferential waves.

2. Results

Results are presented in two parts. The first part discusses static buckling while the second part discusses dynamic divergence from impulsive loading. In all numerical simulations, the disk has a radius $r_d = 3$ in. and thickness $h = 0.1$, 0.2 or 0.3 in. The disk is forced by a uniform concentric pressure acting over a circle of radius $r_p = 0.2$ or 0.5 in. The (h, r_p) dyad for each of the six cases is listed in Table 1.

For flexural motions of the disk, the perimeter is simply supported, i.e. $M_{rr}(r_d) \equiv \psi_\theta(r_d) \equiv w(r_d) = 0$ (see Eq. (B.24b)). For motions in the plane of the disk, the perimeter is stress free, i.e. $\sigma_{r0}(r_d) = 0$. The material properties of the disk are

$$E = 45 \times 10^6 \text{ lb/in.}^2, \quad \rho = 3 \times 10^{-4} \text{ lb s}^2/\text{in.}^4, \quad \nu = 0.25 \tag{25}$$

The prebuckling static axisymmetric flexural response is computed by the exact solution derived in Appendix A. Displacement and its derivatives are then used to compute $W_0(r)$ in Eqs. (9a) and (9b) yielding the induced stresses in the plane of the disk. For $p_0 = 1$, the distribution along r of $(\sigma_{r0}, \sigma_{\theta 0})$ for cases 1, 2, 3 and 5 in Table 1 are shown in Fig. 1(a–d). Note that for all cases $\sigma_{\theta 0}$ turns negative near $r/r_d = 0.43$, and that the functional form of $(\sigma_{r0}, \sigma_{\theta 0})/\sigma_{\max}$ is as predicted by the simpler one term solution in Eqs. (12a)–(12e), independent of h and r_p.

The transition of $\sigma_{\theta 0}$ from positive near disk center to negative near the perimeter can be explained in two ways. The first relies on the mathematical form of the constituents in Eq. (9d) rewritten below for convenience

$$\sigma_{\theta 0}(r) = \frac{E}{1-\nu^2}\left\{ -\frac{(1-\nu)}{r^2}\int_0^r \eta \int_0^\eta W_0(\xi)\,\mathrm{d}\xi\,\mathrm{d}\eta - \nu \int_0^r W_0(\xi)\,\mathrm{d}\xi + \frac{\nu}{2}(w_0'(r))^2 \right.$$
$$\left. -\frac{(1-\nu)}{r_d^2}\int_0^{r_d} \eta \int_0^\eta W_0(\xi)\,\mathrm{d}\xi\,\mathrm{d}\eta + \int_0^{r_d} W_0(\xi)\,\mathrm{d}\xi - \frac{1}{2}(w_0'(r_d))^2 \right\} \quad \text{(see (9d))}$$

Since $W_0(\xi)$ is positive definite as evidenced from Eq. (7b), it is clear that in Eq. (9d) the groups formed by terms (1,4) and (3,6) are negative definite and the group formed by terms (2,5) is positive definite. At $r = 0$, the first three terms in (9d) vanish because the upper limit of the integrals is zero, and $w_0'(0) = 0$ from axisymmetry. Since

$$\frac{(1-\nu)}{r_d^2}\int_0^{r_d} \eta \int_0^\eta W_0(\xi)\,\mathrm{d}\xi\,\mathrm{d}\eta < \frac{(1-\nu)}{2}\int_0^{r_d} W_0(\xi)\,\mathrm{d}\xi \quad \text{and} \quad \int_0^{r_d} W_0(\xi)\,\mathrm{d}\xi > \frac{1}{2}(w_0'(r_d))^2$$

Table 1
h and r_p for cases 1–6

Case	h (in.)	r_p (in.)
1	0.1	0.2
2	0.2	0.2
3	0.3	0.2
4	0.1	0.5
5	0.2	0.5
6	0.3	0.5

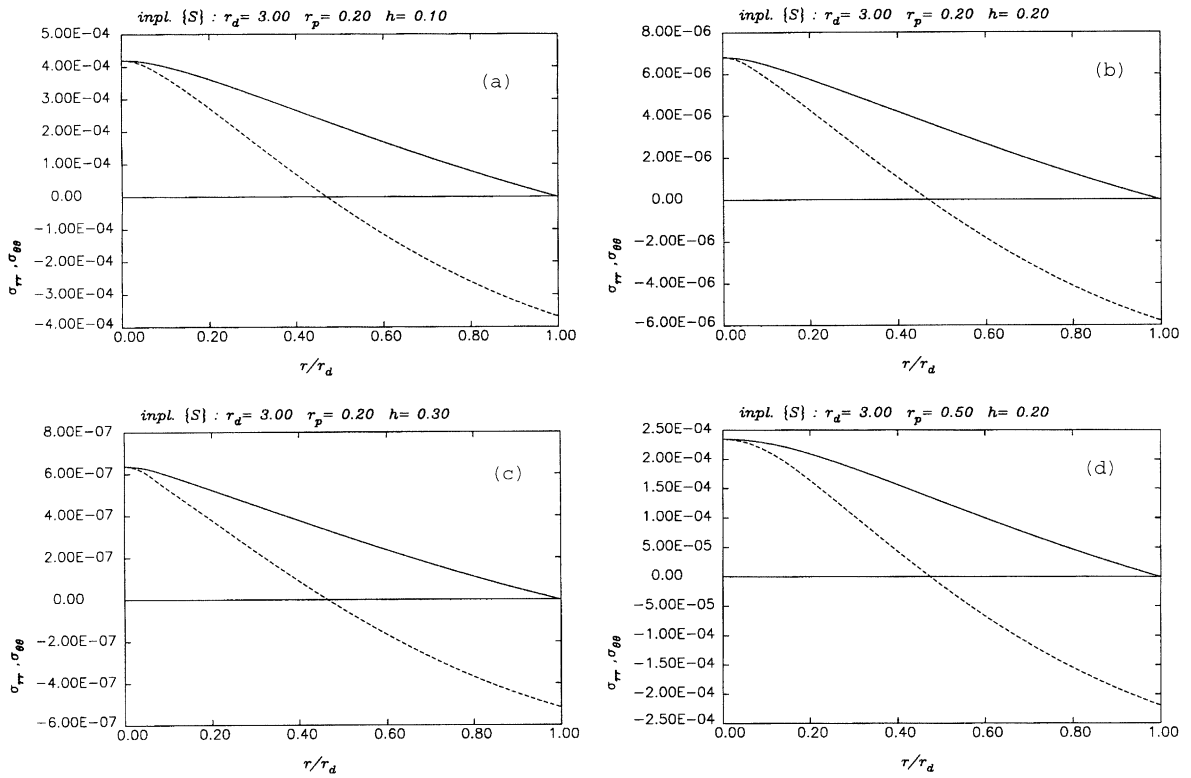

Fig. 1. Radial distribution of static inplane $(\sigma_{r0}, \sigma_{\theta 0})$.

then $\sigma_{\theta 0}(0)$ satisfies the inequality

$$\sigma_{\theta 0}(0) > \frac{E}{(1-v^2)}\left\{\frac{(1+v)}{2}\int_0^{r_\mathrm{d}} W_0(\xi)\,\mathrm{d}\xi - \frac{(1-v)}{2}\left(w_0'(r_\mathrm{d})\right)^2\right\}$$

and is positive definite. Based on the same approximations above, $\sigma_{\theta 0}(r_\mathrm{d})$ reduces to

$$\begin{aligned}\sigma_{\theta 0}(r_\mathrm{d}) &< \frac{E}{(1-v^2)}\left\{-(1-v)\int_0^{r_\mathrm{d}} W_0(\xi)\,\mathrm{d}\xi + (1-v)\int_0^{r_\mathrm{d}} W_0(\xi)\,\mathrm{d}\xi - \frac{(1-v)}{2}\left(w_0'(r_\mathrm{d})\right)^2\right\}\\ &< -\frac{E}{2(1+v)}\left(w_0'(r_\mathrm{d})\right)^2\end{aligned}$$

which is negative definite.

The other way to explain the transition is from physical grounds. Consider an unconstrained thin disk resting on a frictionless ring near the disk boundary. A concentrated force applied at the center of the disk produces axial deformation from flexure and radial deformation towards the center to compensate for an almost constant intrinsic length of the disk $\int_0^r (1+(w_0')^2)^{1/2}\,\mathrm{d}r$. This means that the radial station on the disk at the supporting ring slides inward. The difference in length of perimeters at the support between undeformed and deformed shapes accounts for the compressive $\sigma_{\theta 0}$.

For each n, expanding w_n according to Eqs. (12a)–(12e) including the first five radial wave numbers yields the eigenmatrix in Eqs. (14a)–(14d). Its solution determines $p_\mathrm{cr}(n)$. Fig. 2(a–d) plots p_cr versus n for

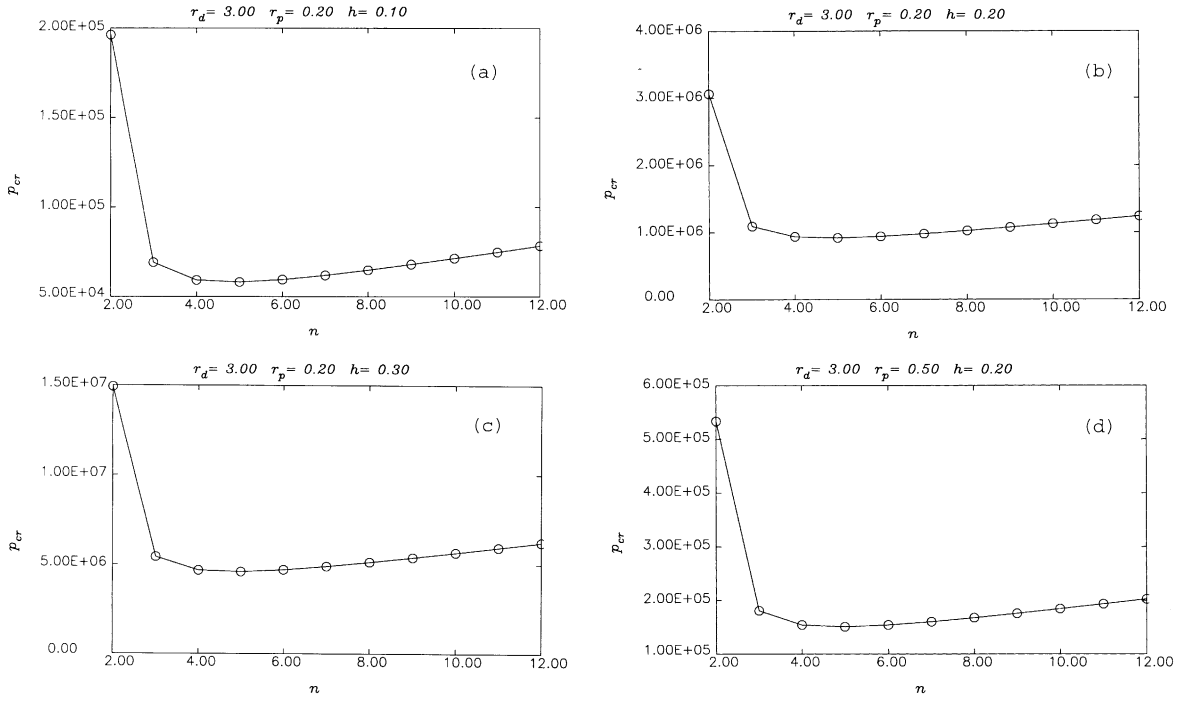

Fig. 2. Variation of static p_{cr} with n.

cases 1, 2, 3 and 5. Note that all cases share the following characteristics independent of h and r_p; p_{cr} falls steeply between $n = 2$ and 3, reaches a minimum at $n = 5$ then rises slowly for $n > 5$. In fact this result agrees with that in Section 1.1 using the one-term approximation for w_n. This insensitivity to h and r_p of n_{cr} follows that of $(\sigma_{r0}, \sigma_{\theta 0})/\sigma_{max}$ depicted in Fig. 1(a–d). This suggests that $(\sigma_{r0}, \sigma_{\theta 0})/\sigma_{max}$ control the shape of the buckling mode. To explain this behavior, refer to Eq. (7b) governing inplane motion of the disk. The functional form of u_0 depends only on $W_0(w_0, w_0', w_0'')$, while the functional forms of w_0, w_0', w_0'' are independent of h (see Eqs. (A.4a) and (A.5a)) and depend weakly on r_p for $r_p \ll r_d$. Since buckling is controlled by the negative portion of $\sigma_{\theta 0}$ in W_0 where W_0 is almost independent of r_p, this explains the insensitivity to r_p of the functional form of $\sigma_{\theta 0}$. Finally, the magnitude of $(p_{cr})_{min}$ for each of the cases in Fig. 1 matches the scaling law in Eq. (11) closely.

In the dynamic case, the time shape of the forcing pulse is assumed trapezoidal with a duration of 50 μs, and rise and fall times of 5 μs. Dynamic instability is fundamentally different from static buckling in the following ways. Static buckling presumably happens instantaneously, and critical pressure p_{cr} is determined uniquely by the solution of an eigenvalue problem, yielding a buckling mode independent of geometry. Dynamic instability depends on the evolution with time of asymmetric displacement induced by imperfections in loading and geometry which increase with time while the forcing pulse is acting. The deformed shape is confined by the shear wave front which propagates at the instantaneous shear wave speed. Flexural deformation w_0 induces inplane stresses that rise concomitantly. As with static buckling, the negative portion of $\sigma_{\theta 0}$ reduces stiffness and a time is reached when the lowest eigenvalue vanishes to become negative afterward. This marks the start of divergence. Other higher frequency modes then follow the same path also becoming unstable while the forcing pulse is acting. To reach this level requires a minimum pressure threshold and/or a maximum disk thickness which is the measure of stiffness provided material

properties are fixed. Unlike the static case where flexural deformation produces inplane stresses instantaneously, in the dynamic case, the process is modulated by radial wave propagation of the disk. This added freedom suggests that the radial distribution of $(\sigma_{r0}, \sigma_{\theta 0})$ will differ substantially from the corresponding static distribution in Fig. 1.

An axisymmetric load acting on an axisymmetric geometry cannot excite asymmetric modes. The only possible process is by small asymmetries from loading and geometric imperfections which magnify in time because of the divergence explained above. Loading imperfections result from asymmetry in spatial pressure distribution or eccentricity. If eccentricity is small compared to disk radius, the generalized force from loading asymmetry affects only modes with low n. This is because $\varphi_n(r)$ for $n \geqslant 2$ becomes negligibly small near $r = 0$. Since generalized force is the inner product $\langle p | r\varphi_n \rangle$ over the foot-print, it in turn will be correspondingly small. On the other hand, generalized force from initial geometric imperfection is similar in form to geometric stiffness which is the inner product $\langle \boldsymbol{\sigma}_0 \cdot \boldsymbol{\kappa}_i | r\varphi_n \rangle$ where $\boldsymbol{\sigma}_0 = \{\boldsymbol{\sigma}_{r0}, \boldsymbol{\sigma}_{\theta 0}\}^{\mathrm{T}}$ and $\boldsymbol{\kappa}_i$ is vector of curvature from initial imperfection w_{i} in Eq. (5). Since geometric imperfection usually spreads over the whole disk, the resulting generalized force is finite for all n. In the analysis to follow, magnitude of imperfections is assumed to be $\varepsilon_p = 0.1$ lb/in.^{2} and $\varepsilon_w = 0.01''$. Both types are constant for all n to avoid any bias for or against a specific n.

For $n = 5$, Fig. 3 shows the evolution of the eigenvalues ω_{mn} of the first five radial modes m for cases 1, 3 and 5 in Table 1. For each case, the value of $p_{\max}$ is listed in Table 2. $p_{\max}$ produces sufficient negative $\sigma_{\theta 0}$ after 25 μs from impact, to cause an unstable asymmetric flexural stress $\sigma_{\theta n}$ to grow by two orders of magnitude from the initial axisymmetric flexural stress $\sigma_{\theta 0}$. For case 1 (Fig. 3(a)), ω_{mn} turns negative in an ascending order of m and maintains its negative value even after the 50 μs pulse has elapsed. In case 3

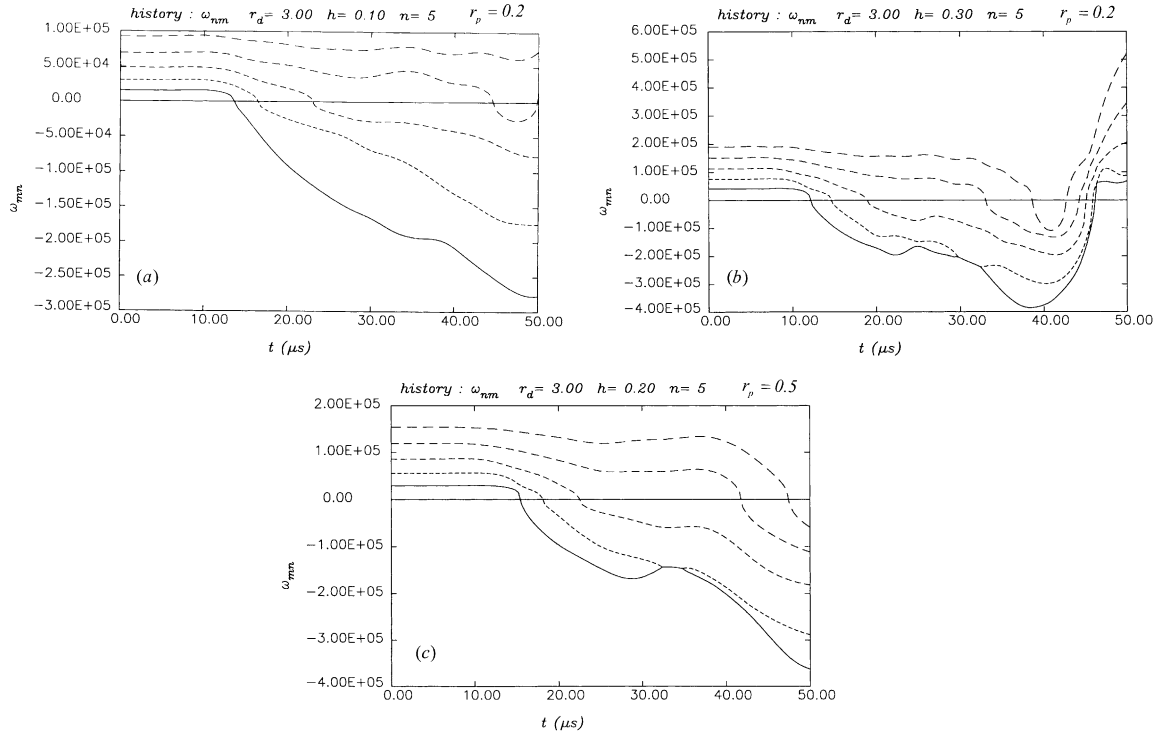

Fig. 3. Evolution of ω_{mn} with time for cases 1, 3 and 5.

Table 2
$p_{\mathrm{cr\,stat}}$ and $p_{mx\,\mathrm{dyn}}$ in psi for cases 1–7

Case	h (in.)	r_p (in.)	$p_{\mathrm{cr\,stat}}$	$p_{mx\,\mathrm{dyn}}$
1	0.1	0.2	5.82E4	1.00E6
2	0.2	0.2	9.20E5	5.00E6
3	0.3	0.2	4.59E6	1.50E7
4	0.1	0.5	9.55E3	2.50E5
5	0.2	0.5	1.51E5	1.00E6
6	0.3	0.5	7.53E5	3.00E6
7	0.4	0.5	2.42E6	6.00E6

(Fig. 3(b)), the thicker disk response stabilizes near 45 μs when the ω_{mn} lines rise back to positive values. Case 5 (Fig. 3(c)) resembles case 1 since stiffening from a thicker disk is counteracted by rise in total load from a wider r_p.

Fig. 4(a–c) show snap-shots in time of instantaneous distribution along r of $(\sigma_{r0}, \sigma_{\theta 0})$. At $t = 5$ μs, the shear wave front is at $r = 1$ in. explaining the vanishing $(\sigma_{r0}, \sigma_{\theta 0})$ for $r > 1$ in. For $t = 15$ μs, the front reaches $r = 2$ in. while w_0 increases, inducing higher $(\sigma_{r0}, \sigma_{\theta 0})$. At $t = 25$ μs, the front reaches $r = r_{\mathrm{d}}$ and reflects back to the center. In contrast to the static distributions in Fig. 1, both σ_{r0} and $\sigma_{\theta 0}$ in Fig. 4 reach largest negative magnitudes at r stations closer to the center.

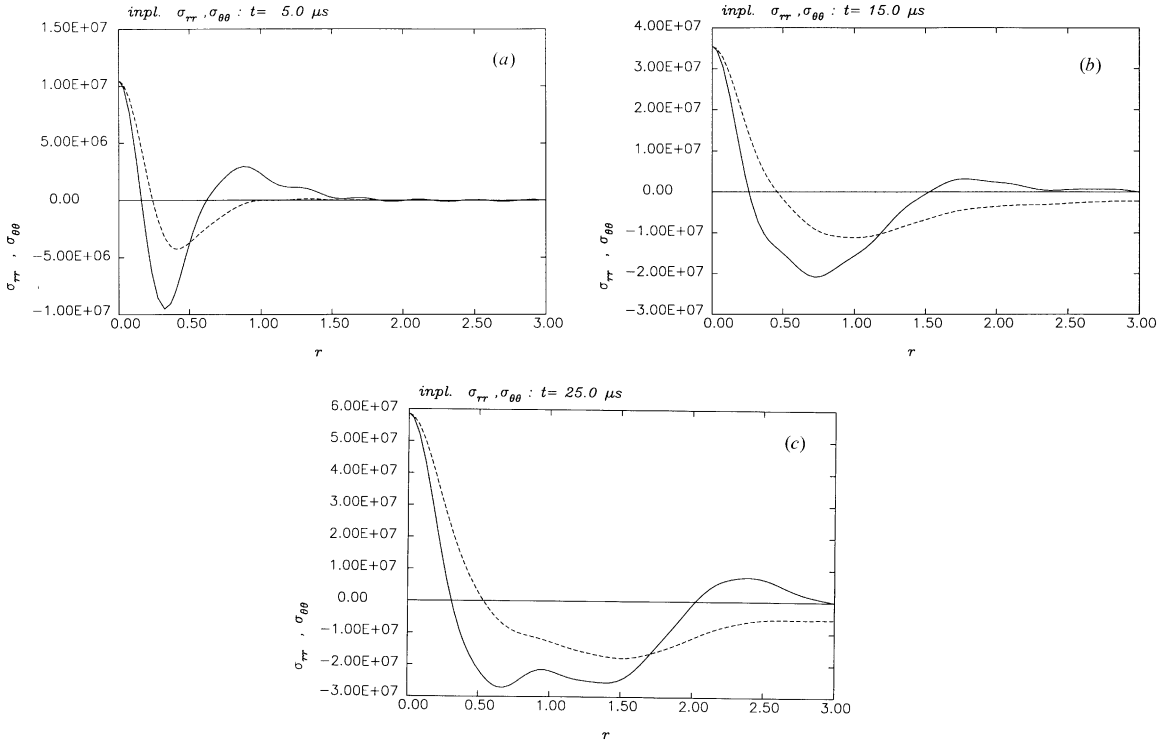

Fig. 4. Snap-shots of $(\sigma_{r0}, \sigma_{\theta 0})$ along r for case 3 at $t = 5$, 15 and 25 μs.

The unstable growth of $\sigma_{\theta n}$ is found by integrating Eqs. (22a) and (22b) numerically. For each n, the integration is stopped at $t = 25$ μs and the maximum value of $\sigma_{\theta n}$ over the disk's surface is termed $\sigma_{\theta n\max}$. A plot of $\sigma_{\theta n\max}$ versus n reveals a maximum at some $n_{\rm cr}$ related to the critical asymmetric mode causing failure of the material by $2n_{\rm cr}$ radial cracks and as many circumferential cracks as the dominant radial wave number of the $n_{\rm cr}$ mode. Fig. 5(a–c) plot $\sigma_{\theta n\max}$ versus n for cases 1, 2 and 3. For fixed r_p, $n_{\rm cr}$ rises with h. An explanation is that for a thicker disk, lines of ω_{mn} versus n and fixed m are flatter than those of a thinner disk, allowing higher n modes to be excited. Fig. 6(a–d) plot $\sigma_{\theta\theta\max}$ versus n for cases 4, 5, 6 and 7 (see Table 2). Comparing plots in Fig. 5 to those in Fig. 6 for the same h reveals that $n_{\rm cr}$ rises with r_p. One explanation is that $(\sigma_{r0}, \sigma_{\theta 0})$ turns negative at larger r when r_p rises and this in turn increases $\langle \boldsymbol{\sigma}_0 \cdot \boldsymbol{\kappa}_t | r\boldsymbol{\varphi}_n \rangle$ at the higher n to compensate for the vanishingly small φ_n near $r = 0$.

The effect of rise time of the forcing pulse $t_{\rm rise}$ is demonstrated by Fig. 7(a–c). Case 2 was recomputed for $t_{\rm rise} = 2.5$, 5 and 10 μs using the same $p_{\max}$ for that case in Table 2. Although $t_{\rm rise}$ has no effect on $n_{\rm cr}$, a shorter $t_{\rm rise}$ intensifies the instability by raising $\sigma_{\theta n\max}$, while a longer $t_{\rm rise}$ has the reverse effect. Finally, if $p_{\max}$ equals the static $p_{\rm cr}$ listed in Table 2, no instability will occur at least during the duration of the pulse. This suggests that higher pressure is needed for dynamic instability than for static buckling, i.e. $p_{\max\ {\rm dyn}} > p_{{\rm cr\ stat}}$. One explanation is that a dynamic load has to overcome stiffness as well as inertia, while the later is absent in the static case.

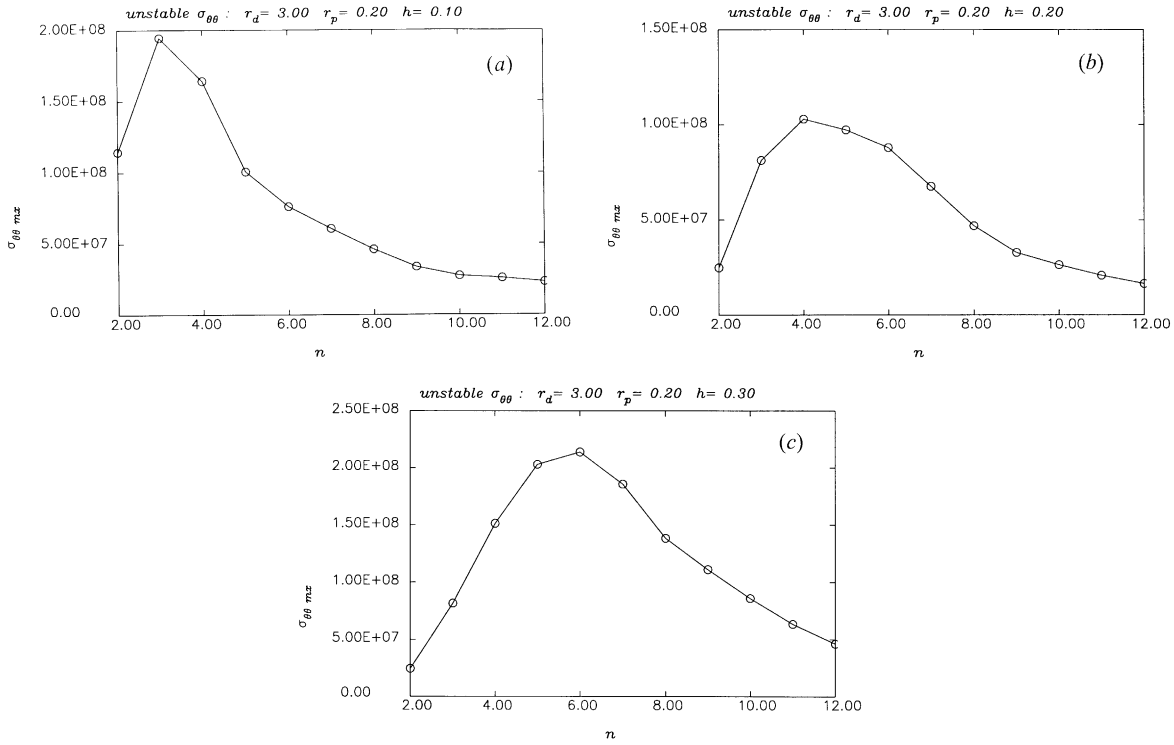

Fig. 5. Variation of $\sigma_{\theta n\max}$ with n for cases 1, 2, 3.

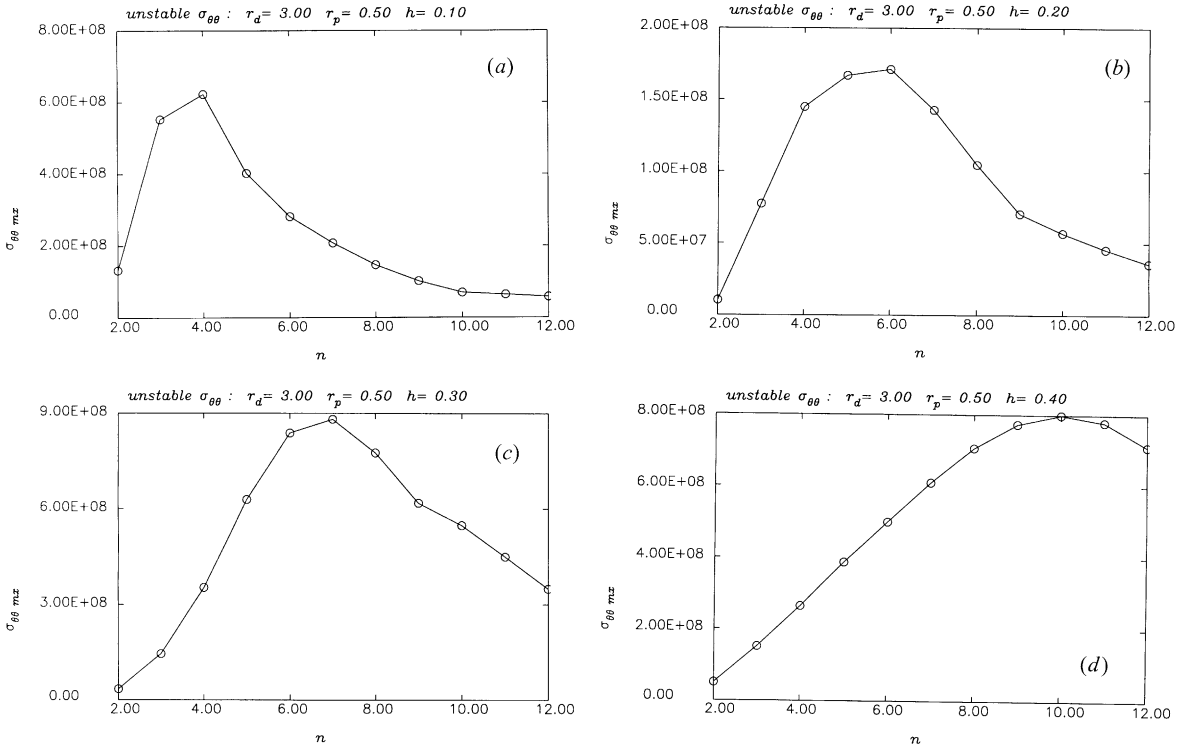

Fig. 6. Variation of $\sigma_{\theta n\max}$ with n for cases 4, 5, 6, 7.

3. Conclusion

Static buckling and dynamic instability of a thin disk were analyzed by a linearized perturbation procedure. Noteworthy results are listed below:

For static buckling:

1. p_{cr} follows a scaling law proportional to $Eh^4/(r_d r_p)^2$.
2. The radial distribution $(\sigma_{r0}, \sigma_{\theta 0})$ induced by the prebuckling axisymmetric flexural deformation w_0, and the corresponding asymmetric buckling mode are insensitive to all parameters.
3. p_{cr} drops sharply from $n = 2$ to $n = 3$, achieves a minimum at $n_{cr} = 5$, then rises smoothly for $n > 5$.
4. n_{cr} is independent of h/r_d and r_p/r_d because the functional form of the solution is independent of these parameters.

For dynamic instability including effects of radial propagation:

1. Confined by the shear wave front, w_0 induces $(\sigma_{r0}, \sigma_{\theta 0})$ whose radial distribution changes substantially with time.
2. The negative portions of $(\sigma_{r0}, \sigma_{\theta 0})$ cause instability by changing the sign of the eigenvalues, creating negative geometric stiffness.
3. Asymmetric initial imperfections in loading and geometry diverge with time if p_{max} is sufficiently high.

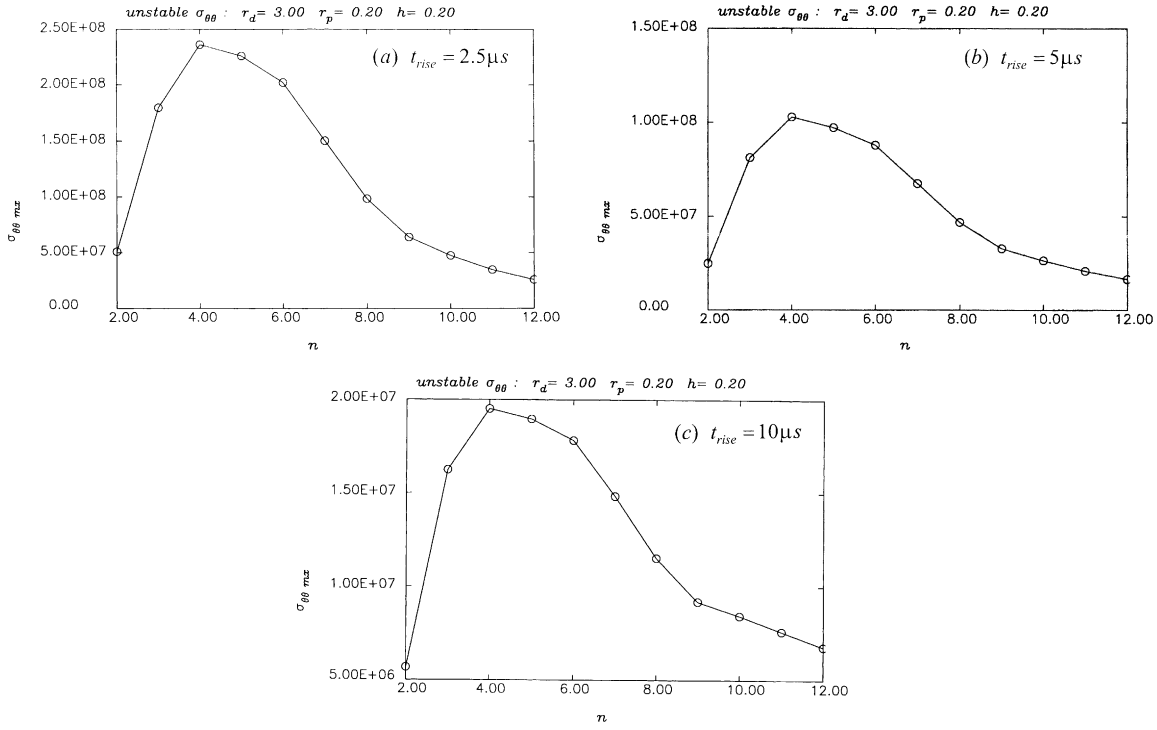

Fig. 7. Effect of t_{rise} on $\sigma_{\theta n\max}$ for case 2.

4. That asymmetric mode growing fastest and reaching the largest magnitude of $\sigma_{\theta n\max}$ over a finite time interval from impact is the critical unstable mode for that n.
5. $\sigma_{\theta n\max}$ varies smoothly with n and reaches a maximum at some n_{cr}.
6. Unlike static buckling, n_{cr} increases with h and r_p, but is insensitive to t_{rise} when $t_{\text{rise}} < 2\pi/\omega_{1,n}$.
7. Reducing t_{rise} strengthens the instability yielding a higher $\sigma_{\theta n\max}$ for the same $p_{\max}$.
8. The threshold of $p_{\max}$ causing dynamic instability during the time interval of the forcing pulse is substantially higher than static p_{cr}, because of inertia opposing motion, and the shift in largest negative magnitude of $\sigma_{\theta 0}$ toward the center where a higher pressure is needed to cause instability.

Appendix A. Axisymmetric static response

The static axisymmetric Mindlin's equations for a disk are

$$D\nabla_1^2\psi_r - \kappa Gh\left(\frac{\partial w}{\partial r} + \psi_r\right) = 0 \tag{A.1}$$

$$\kappa Gh\left(\nabla_0^2 w + \frac{1}{r}\frac{\partial}{\partial r}(r\psi_r)\right) = -p[H(r) - H(r - r_p)] + p_{\text{b}} \tag{A.2}$$

where (ψ_r, w) are rotation and axial displacement, G is shear modulus, κ is shear constant, p is uniform pressure acting over $0 \leqslant r \leqslant r_p$, and p_{b} is uniform pressure over $0 \leqslant r \leqslant r_{\text{d}}$, opposing p with magnitude

$p_b = p(r_p/r_d)^2$ to equilibrate the disk when the boundary is stress-free. Eliminating ψ_r from (A.2) using (A.1) yields

$$\nabla_0^4 w = \frac{1}{D}\{p[H(r) - H(r - r_p)] - p_b\} \tag{A.3}$$

To solve (A.3) analytically, divide the disk into two parts. The first is a solid disk in $0 \leqslant r \leqslant r_p$ forced by $(p - p_b)$, and the second is an annular disk $r_p \leqslant r \leqslant r_d$ forced by $-p_b$. Integrating (A.3) then (A.2) in parts 1 and 2 produces

$$w_1(r) = C_1 r^2 + C_2 + \frac{(p - p_b)}{64D} r^4 \tag{A.4a}$$

$$\psi_{r1}(r) = -2C_1 r - \frac{(p - p_b)}{2\kappa Gh} r - \frac{(p - p_b)}{16D} r^3 \tag{A.4b}$$

$$Q_{r1}(r) = -\frac{(p - p_b)}{2} r \tag{A.4c}$$

$$M_{r1}(r) = -D\left[2(1 + v)C_1 + \frac{(1 + v)(p - p_b)}{2\kappa Gh} + \frac{(3 + v)(p - p_b)}{16D} r^2\right] \tag{A.4d}$$

where Q_r and M_r are shear and moment resultant.

$$w_2(r) = C_3 r^2 + C_4 r^2 \ell nr + C_5 \ell nr + C_6 - \frac{p_b}{64D} r^4 \tag{A.5a}$$

$$\psi_{r2}(r) = -2C_3 r - C_4 r(2\ell nr + 1) + \frac{C_7}{r} + \frac{p_b r}{2\kappa Gh} + \frac{p_b r^3}{16D} \tag{A.5b}$$

$$Q_{r2}(r) = \frac{\kappa Gh}{r}(C_5 + C_7) + \frac{p_b r}{2} \tag{A.5c}$$

$$M_{r2}(r) = -D\left[2(1 + v)C_3 + C_4(2(1 + v)\ell nr + 3 + v) + \frac{(1 - v)C_7}{r^2} - \frac{(1 + v)p_b}{2\kappa Gh} - \frac{(3 + v)p_b r^2}{16D}\right] \tag{A.5d}$$

C_7 can be expressed in terms of C_j, $j = 4, 5$ by substituting (A.5a) and (A.5b) in (A.1) then equating coefficients of each primitive to zero

$$C_7 = -\left[\frac{2h^2}{3(1 - v)k} C_4 + C_5\right] \tag{A.6}$$

Coefficients C_j, $j = 1, 7$ are determined by enforcing continuity of the state vector $\{Q_r, M_r, w, \psi_r\}^T$ at $r = r_p$ and boundary conditions at $r = r_d$. For simple supports

$$M_{r2}(r_d) \equiv w_2(r_d) = 0 \tag{A.7a}$$

And for stress free

$$M_{r2}(r_d) \equiv Q_{r2}(r_d) = 0 \tag{A.7b}$$

This produces the simultaneous equations

$$\mathbf{M_S C} = \mathbf{P} \tag{A.8}$$

For a solid disk forced by a uniform pressure

$$w_0 = C_1 r^2 + C_2 + pr^4/64D \tag{A.9}$$

For simple supports $w_0(r_d) = 0$, $M_r(r_d) = 0$

$$C_1 r_d^2 + C_2 = -\frac{pr_d^4}{64D}, \quad D = \frac{Eh^3}{12(1-v^2)} \tag{A.10}$$

$$2(1+v)C_1 = -\frac{(1+v)p}{2\kappa Gh} - \frac{(3+v)pr_d^2}{16D}$$

$$\Rightarrow C_1 = -\frac{p}{4\kappa Gh} - \frac{(3+v)pr_d^2}{32(1+v)D}$$

$$C_2 = \frac{pr_d^4}{64D}\left(\frac{5+v}{1+v}\right) + \frac{pr_d^4}{4\kappa Gh^3}\left(\frac{h}{r_d}\right)^2$$

Substituting (A.10) in (A.9) yields

$$\begin{aligned} w_0(r) &= -\left[\frac{pr_d^4(3+v)}{32(1+v)D} + \frac{pr_d^2}{4\kappa Gh}\right]\xi^2 + \frac{pr_d^4}{64D}\left(\frac{5+v}{1+v}\right) + \frac{pr_d^2}{4\kappa Gh} + \frac{pr_d^4}{64D}\xi^4 \\ &= \frac{pr_d^4}{64D}\left[\xi^4 - \frac{2(3+v)}{(1+v)}\xi^2 + \frac{(5+v)}{1+v}\right] + \frac{pr_d^4}{4\kappa Gh^3}(1-\xi^2)\left(\frac{h}{r_d}\right)^2 \end{aligned} \tag{A.11}$$

where $\xi = r/r_d$. In this case, functional form of the solution as defined in Eq. (11) depends on (h/r_d) through shear deformations and is of the order $o(h/r_d)^2$.

In the case when w_0 is approximated by $J_0(k_0 r)$

$$w_0(r) = \frac{pr_d^4}{D}\frac{\eta}{\gamma_{01}^4}J_0(\gamma_{01}\xi), \quad \eta = \frac{\int_0^1 J_0(\gamma_{01}\xi)\xi\,d\xi}{\int_0^1 J_0^2(\gamma_{01}\xi)\xi\,d\xi}, \quad J_0(\gamma_{01}) = 0 \tag{A.12}$$

Note that functional form of (A.12) is independent of h/r_d.

For the case when $p(r) = pr^m[H(r) - H(r - r_p)]$, Eqs. (A.4a)–(A.4d) become

$$w_1(r) = C_1 r^2 + C_2 + \frac{p}{D}\left[\frac{r^{m+4}}{(m+4)^2(m+2)^2} - \frac{\zeta r^{m+2}}{(m+2)^2}\right], \quad \zeta = \frac{h^2}{6(1-v^2)\kappa} \tag{A.13a}$$

$$\psi_{r1}(r) = -2C_1 r - \frac{p}{D}\frac{r^{m+3}}{(m+4)(m+2)^2} \tag{A.13b}$$

$$Q_{r1}(r) = -\frac{p}{(m+2)}r^{m+1} \tag{A.13c}$$

$$M_{r1}(r) = -2D(1+v)C_1 - \frac{(m+3+v)p}{(m+4)(m+2)^2}r^{m+2} \tag{A.13d}$$

Appendix B. Asymmetric eigenproblem

Mindlin's plate equations may be written in vector form as

$$\frac{D}{2}[(1-v)\nabla^2\boldsymbol{\Psi} + (1+v)\nabla\boldsymbol{\Phi}] - \kappa Gh(\boldsymbol{\Psi} + \nabla w) = \frac{\rho h^3}{12}\frac{\partial^2\boldsymbol{\Psi}}{\partial t^2} \tag{B.1}$$

$$\kappa Gh(\nabla^2 w + \boldsymbol{\Phi}) + p = \rho h \frac{\partial^2 w}{\partial t^2} \tag{B.2}$$

$$\boldsymbol{\Phi} = \boldsymbol{\nabla} \cdot \boldsymbol{\Psi}, \quad D = \frac{Eh^3}{12(1-v^2)}$$

where $\boldsymbol{\Psi}$ is the vector of rotations, w is transverse displacement, (ρ, v) are density and Poisson ratio, (E, G) are Young's and shear moduli, κ is shear constant, h is thickness, t is time, p is applied pressure, ∇^2 is the Laplacian and ∇ is the gradient operator. Taking the divergence of (B.1)

$$D\nabla^2 \boldsymbol{\Phi} - \kappa Gh(\boldsymbol{\Phi} + \nabla^2 w) = \frac{\rho h^3}{12} \frac{\partial^2 \boldsymbol{\Phi}}{\partial t^2} \tag{B.3}$$

Eliminating $\boldsymbol{\Phi}$ from (B.2) and (B.3)

$$\left[\left(\nabla^2 - \frac{1}{c_\varepsilon^2}\frac{\partial^2}{\partial t^2}\right)\left(\nabla^2 - \frac{1}{c_s^2}\frac{\partial^2}{\partial t^2}\right) + \frac{12}{c_\varepsilon^2 h^2}\frac{\partial^2}{\partial t^2}\right] w = \left[\frac{1}{D} - \frac{1}{\kappa Gh}\left(\nabla^2 - \frac{1}{c_\varepsilon^2}\frac{\partial^2}{\partial t^2}\right)\right] p \tag{B.4}$$

$$c_\varepsilon^2 = \frac{E}{\rho(1-v^2)}, \quad c_s^2 = \frac{\kappa G}{\rho}$$

Eliminating $\nabla^2 w$ from (B.2) and (B.3) yields

$$\left[D\nabla^2 - \frac{\rho h^3}{12}\frac{\partial^2}{\partial t^2}\right]\boldsymbol{\Phi} = \rho h \frac{\partial^2 w}{\partial t^2} - p \tag{B.5}$$

Taking the curl of (B.1)

$$\left[\frac{D}{2}(1-v)\nabla^2 - \kappa Gh - \frac{\rho h^3}{12}\frac{\partial^2}{\partial t^2}\right](\boldsymbol{\nabla} \times \boldsymbol{\Psi}) = \mathbf{0} \tag{B.6}$$

from which it can be inferred that $(\boldsymbol{\nabla} \times \boldsymbol{\Psi})$ is not a function of w while $\boldsymbol{\Psi}$ may actually be expressed as

$$\boldsymbol{\Psi} = \nabla[g(w)] + \boldsymbol{\nabla} \times \boldsymbol{\Gamma} \tag{B.7}$$

where $\boldsymbol{\Gamma}$ is a vector potential for $\boldsymbol{\Psi}$ independent of w. Substituting (B.7) in (B.5) using the definition of $\boldsymbol{\Phi}$ yields

$$\left[D\nabla^2 - \frac{\rho h^3}{12}\frac{\partial^2}{\partial t^2}\right]\nabla^2 g = \rho h \frac{\partial^2 w}{\partial t^2} - p \tag{B.8}$$

Substituting (B.7) in (B.6) using the identity

$$\nabla \times \nabla \times \mathbf{A} = \nabla(\nabla \cdot \mathbf{A}) - \nabla^2 \mathbf{A} \tag{B.9}$$

produces

$$\left[\frac{D}{2}(1-v)\nabla^2 - \kappa Gh - \rho\frac{h^3}{12}\frac{\partial^2}{\partial t^2}\right]\nabla^2 \boldsymbol{\Gamma} = 0 \tag{B.10}$$

Defining $\boldsymbol{\tau} = \nabla^2 \boldsymbol{\Gamma}$, reduces (B.10) to

$$\left[\nabla^2 - \frac{12\kappa}{h^2} - \frac{2}{(1-v)c_\varepsilon^2}\frac{\partial^2}{\partial t^2}\right]\boldsymbol{\tau} = \mathbf{0} \tag{B.11}$$

For a solid disk and periodic motions in time with frequency ω, the homogeneous solution of (B.4) takes the form

$$w(r,\theta,t) = w(r)\cos n\theta\, e^{i\omega t} \tag{B.12a}$$

$$w(r) = C_1 J_n(k_1 r) + C_2 J_n(k_2 r) \tag{B.12b}$$

$$k^4 - 2\beta_1 k^2 + \beta_2 = 0 \tag{B.12c}$$

$$\beta_1 = \frac{1}{2}\frac{c_\varepsilon^2 + c_s^2}{c_\varepsilon^2 c_s^2}\omega^2, \quad \beta_2 = \frac{\omega^2}{c_\varepsilon^2}\left(\frac{\omega^2}{c_s^2} - \frac{12}{h^2}\right)$$

where (r,θ) are radial and circumferential coordinates, n is circumferential wave number, $i = \sqrt{-1}$. Since g is a function of w, and from (B.8) linear with w, it can be expressed like (B.12a) and (B.12b) as

$$g_j(r) = C_{gj} J_n(k_j r), \quad \nabla^2 g_j = -k_j^2 g_j, \quad j = 1,2 \tag{B.13}$$

Substituting (B.13) in (B.8) yields

$$-\left[-k_j^2 + \frac{\omega^2}{c_\varepsilon^2}\right] k_j^2 C_{gj} = -\frac{12\omega^2}{h^2 c_\varepsilon^2} C_j \tag{B.14}$$

then using (B.4), Eq. (B.14) simplifies to

$$C_{gj} = \frac{1}{k_j^2}\left(-k_j^2 - \frac{\omega^2}{c_s^2}\right) C_j \tag{B.15}$$

Taking the gradient of (B.13)

$$\nabla g_j = \left(\frac{\partial}{\partial r}, -\frac{n}{r}\right) C_{gj} J_n(k_j r) \tag{B.16}$$

Furthermore, since $\boldsymbol{\tau}$ and $\boldsymbol{\Psi}$ are orthogonal, and $\boldsymbol{\Psi}$ is in the plane of the disk then $\boldsymbol{\tau} = (0,0,\tau_z)$ and

$$\tau_z = C_\tau J_n(k_\tau r) \tag{B.17}$$

Substituting (B.17) in (B.11) produces the dispersion relation

$$k_\tau^2 = \frac{2\omega^2}{(1-\nu)c_\varepsilon^2} - \frac{12\kappa}{h^2} \tag{B.18}$$

Eq. (B.18) exhibits a cut-off above

$$\omega_\tau = \sqrt{6\kappa(1-\nu)}\frac{c_\varepsilon}{h} = \frac{\sqrt{12}c_s}{h} \tag{B.19}$$

which is the same as that in (B.12c). Finally, using κ_τ in (B.18) and since $\boldsymbol{\Gamma}$ and $\boldsymbol{\tau}$ are parallel then $\boldsymbol{\Gamma} = (0,0,\Gamma_z)$, and

$$\Gamma_z = C_\Gamma J_n(k_\tau r) \tag{B.20}$$

Taking the curl of (B.20)

$$\nabla \times \boldsymbol{\Gamma} = \left(\frac{n}{r}, -\frac{\partial}{\partial r}\right) C_\Gamma J_n(k_\tau r) \tag{B.21}$$

Substituting (B.16) and (B.21) in (B.7) determines the solutions

$$\psi_r(r,\theta,t) = \cos n\theta\, e^{i\omega t}\left\{\sum_{j=1}^{2} C_{gj} k_j J_n'(k_j r) + \frac{n}{r} C_\Gamma J_n(k_\tau r)\right\} \tag{B.22a}$$

$$\psi_\theta(r,\theta,t) = \sin n\theta\, e^{i\omega t}\left\{ \sum_{j=1}^{2} -\frac{n}{r} C_{gj} J_n(k_j r) - k_\tau C_\Gamma J_n'(k_\tau r) \right\} \tag{B.22b}$$

$$w(r,\theta,t) = \cos n\theta\, e^{i\omega t} \sum_{j=1}^{2} C_j J_n(k_j r) \tag{B.22c}$$

where C_{gi} is related to C_i by (B.15).

Moments and shear resultants at the boundary are expressed in terms of (ψ_r, ψ_θ, w) as

$$M_{rr} = D\left[\frac{\partial \psi_r}{\partial r} + v\left(\frac{\psi_r}{r} + \frac{1}{r}\frac{\partial \psi_\theta}{\partial \theta} \right) \right] \tag{B.23a}$$

$$M_{r\theta} = \frac{D(1-v)}{2}\left[\frac{1}{r}\frac{\partial \psi_r}{\partial \theta} + \frac{\partial \psi_\theta}{\partial r} - \frac{\psi_\theta}{r} \right] \tag{B.23b}$$

$$Q_r = \kappa G h\left(\frac{\partial w}{\partial r} + \psi_r \right) \tag{B.23c}$$

For a free edge

$$M_{rr}(r_d) \equiv M_{r\theta}(r_d) \equiv Q_r(r_d) = 0 \tag{B.24a}$$

and for a simply supported edge

$$M_{rr}(r_d) \equiv \psi_\theta(r_d) \equiv w(r_d) = 0 \tag{B.24b}$$

Substituting (B.22a)–(B.22c) in (B.23a)–(B.23c) then in either (B.24a) or (B.24b) produces the implicit eigenvalue problem

$$\mathbf{B}(r_d)\mathbf{C} = 0 \Rightarrow \det|\mathbf{B}| = \mathbf{0} \tag{B.25a}$$

where $\mathbf{B}$ is a 3×3 matrix of the fundamental solutions in (ψ_r, ψ_θ, w) and their first derivatives, and

$$\mathbf{C} = \{C_1, C_2, C_\Gamma\}^T \tag{B.25b}$$

$\{\psi_{rn}, \psi_{\theta n}, w_n\}$ can be expanded in terms of the eigenset $\{\omega_n, \eta_{rn}, \eta_{\theta n}, \varphi_n\}$.

References

Bhushan, B., Singh, G., Rao, G., 1996. Axisymmetric buckling of layered orthotropic circular and annular plates of varying thickness using a computationally economic semi-analytical finite element approach. Computers and Structures 59, 21–33.

Bolotin, B., 1956. Dynamic Stability of Elastic Systems, English translation published by Holden Day.

Chen, L., Juang, D., 1987. Axisymmetric buckling of circular plates. Computers and Structures 25, 175–182.

El-Raheb, M., Wagner, P., 1987. Wave propagation in a plate after impact by a projectile. Journal of Acoustical Society of America 82 (2), 498–505.

Khadkhodayan, M., Zhang, L., Sowerby, R., 1997. Analyses of wrinkling and buckling of elastic plates by DXDR method. Computers and Structures 4, 561–574.

Kolegov, L., Lin, E., Ryazanov, V., Funtikov, A., 1991. Experimental study of the deformation and fracture of circular aluminum plates under the influence of a shock wave. Journal of Applied Mechanics and Technical Physics 32, 906–910.

Krizghevsky, G., Stavsky, Y., 1998. Refined dynamic stability theory of laminated isotropic circular plates. ASME Journal of Applied Mechanics 65, 334–340.

Laura, P., Larrondo, H., Avalos, D., Bambill, D., 1995. Dynamic stiffening of circular plates and determination of their buckling in-plane pressure. Applied Acoustics 44, 125–132.

Nath, Y., Dumir, P., Bhatia, R., 1985. Non-linear static and dynamic analysis of circular plates and shallow spherical shells using the collocation method. International Journal of Numerical Methods in Engineering 21, 565–578.

Shih, W., Kudryavtsev, L., Wang, K., 1995. Elastic buckling of a circular disk due to internal membrane forces. ASME Journal of Applied Mechanics 62, 813–816.

Tani, J., Yamaki, N., 1981. Elastic instability of a uniform compressed annular plate with axisymmetric initial deflection. Journal of Nonlinear Mechanics 16, 213–220.

Timoshenko, S., Woinowsky-Krieger, S., 1959. Theory of Plates and Shells, second ed. McGraw-Hill Book Co., pp. 396–400.

Turvey, G., 1978. Axisymmetric snap buckling of imperfect tapered circular plates. Computers and Structures 9, 551–558.

Yamaki, N., Otomo, K., Chiba, M., 1981. Non-linear vibrations of a clamped circular plate with initial deflection and initial edge displacement; I Theory. Journal of Sound and Vibration 79, 23–42.